NESTOR FACILITY INJECTION CONCEPTION

P. Gladkikh, I. Karnaukhov, A. Mytsykov, V. Skyrda, A. Zelinsky*

National Science Center "Kharkov Institute of Physics and Technology", 61108, Kharkov, Ukraine

(Received April 18, 2011)

During the last years X-ray generator NESTOR is under construction in NSC KIPT. According to the project, 60 MeV electrons are injected in the storage ring and further can be accelerated up to the maximal energy 225 MeV. Due to compact design of the ring, injection trajectory of the beam passes through fringe field of NESTOR bending magnet. It brings additional difficulties of injection system design. In the paper the results of NESTOR facility injection system are presented. The results show that designed system provides matching of injected beam parameters with the storage ring acceptance and is stable to element alignment errors.

PACS: 29.20.D-, 29.20.Ej, 07.85.Fv

1. INTRODUCTION

It is known that injection in a compact storage ring, such as NSC KIPT X-ray source NESTOR [1], is a very difficult task due to very dense facility lattice.

During NESTOR design it was decided to inject electron beam through fringe fields of a bending magnet [2]. In this way one can provide smooth trajectory of injected beam and save room in the ring. But such decision requires few special characteristics of transportation beam line [3].

The second distinction of the NESTOR injection scheme is multiturn injection. After septum injected beam enters the ring in 16 mm away from the design orbit. Further, injected beam damps and another portion of injected beam can be delivered. This scheme demands very careful and accurate design and calculations of the whole beam trajectory as well as of injection devices. To provide successful injection in the ring the acceptable tolerances of the ring magnetic element alignments were determined and injected beam emittance and storage ring acceptance were matched. The designed transportation channel consists of two bending magnets, five-lens asymmetrical objective and two-lens matching cell to compensate dispersion and focusing effects of a dipole magnet fringe field.

Recently it has been decided to use electrical inflector on the running wave as a final beam deflector and power source on the base of SOS diode [4] for it. The electrical inflector has been designed and beam tracing trough fringe fields of the final part of the injection channel considering focusing properties of the newly designed inflector has been simulated.

The paper is devoted to the description of the design conception of NESTOR facility injection system and describes the results of its design and calculations.

2. MAGNETIC ELEMENT ALIGNMENT TOLERANCES

A storage ring NESTOR has racetrack like lattice [1]. The lattice consists of 4 bending magnets, 20 quadrupole magnets 18 sextupole magnets partly with octupole field component. A large number of focusing electromagnetic elements and presence of low-β sections demand very strict requirements to the accuracy of lattice element alignment. Reference orbit (RO) distortions have to allow electron beam injection in the storage ring and further RO corrections. To determine the effect of displacements of different types of the magnetic elements on value of RO distortions we have calculated RO coordinates with displacements of quadrupoles and bending magnets separately.

As simulations results have shown the effect of quadrupole lens tilts is much less then effect of lens displacements. Results of RO numerical simulations at Gaussian distribution of alignment errors of quadrupole lenses with RMS value of alignment errors equal to Δz=100 μm are shown in Fig.1,2. Fig.1 shows distribution of maximal RO distortions depends on RMS value of alignment tolerance. Fig.2 presents dependence of maximum value of RMS RO distortions on RMS value of alignment tolerance. As calculations showed, the strong lenses of final triplets make the main contribution in RO distortions due to quadrupole lenses misalignments. It can be illustrated with Fig.3,4 were the RMS values of RO distortions along NESTOR storage ring due to regular part (see Fig.3) and final triplet (see Fig.4) quadrupole lens displacements of Δz=100 μm RMS value are depicted.

In similar manner the calculations of RO distortions due to bending magnet misalignments in all planes were carried out (see Fig.5).

*Corresponding author E-mail address: zelinsky@kipt.kharkov.ua

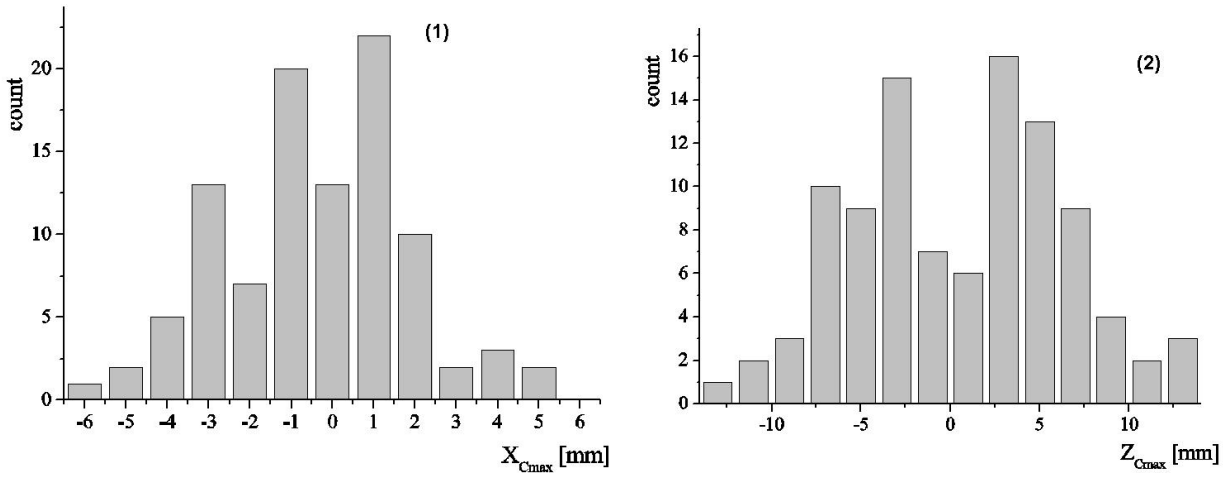

Fig.1. *Distribution of maximal value of RO distortions at RMS quadrupole misalignments $\Delta x = 100\,\mu m$, 1 - horizontal plane, 2 - vertical plane*

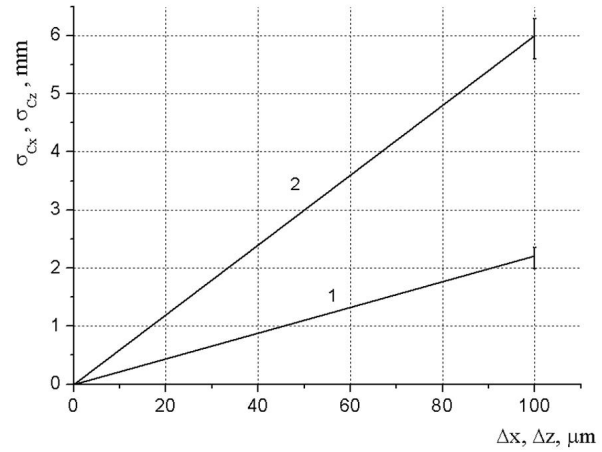

Fig.2. *RMS value of maximal RO distortions vs RMS value of quadrupole misalignments in horizontal (1) and vertical (2) planes*

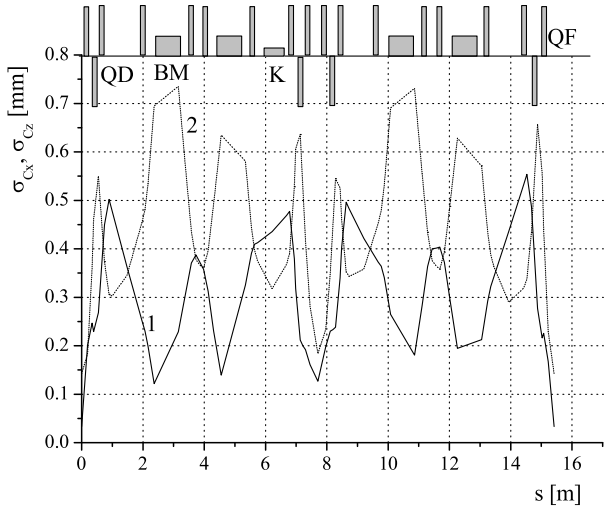

Fig.3. *RMS values of RO distortions along NESTOR storage ring due to regular part quadrupole lense displacements of $\Delta x = \Delta z = 100\,\mu m$, 1 - horizontal plane, 2 - vertical plane*

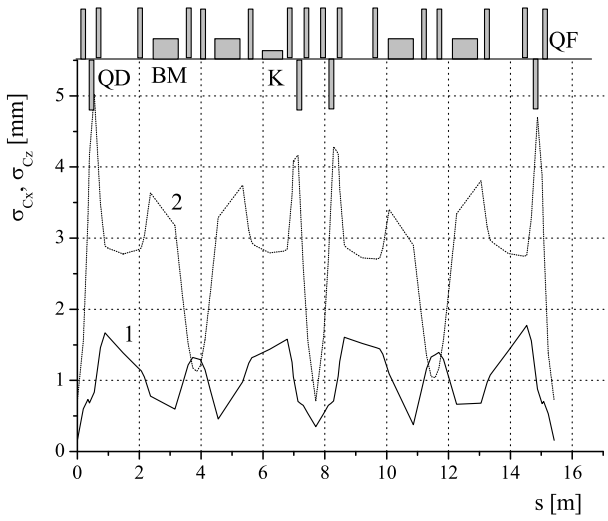

Fig.4. *RMS values of RO distortions along NESTOR storage ring due to final triplet quadrupole lense displacements of $\Delta x = \Delta z = 100\,\mu m$, 1 - horizontal plane, 2 - vertical plane*

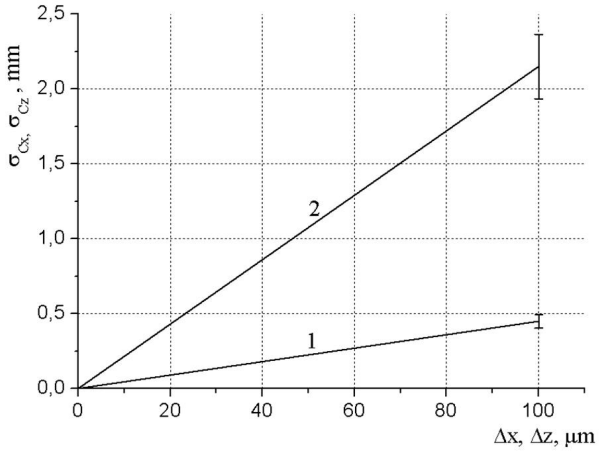

Fig.5. *RMS value of maximal RO distortions vs RMS value of bending magnet misalignments in horizontal (1) and vertical (2) planes*

As it is clear from the Fig.1,2 the contribution of quadrupole lenses in total RO distortion is much bigger compare to bending magnets misalignment effect. The accuracy of equipment alignment relative to vertical axis is determined by accuracy of plane measurements and length of elements. For bending magnets it is $a_{sx} \sim 2.5 \times 10^{-4}$, and for quadrupoles $a_{sx} \sim 2.5 \times 10^{-3}$.

Dependences of RO distortions presented above determined the plane and angular magnetic element alignment tolerances of bending magnet and quadrupoles of the storage ring equal to $\Delta z = \Delta x = 100\,\mu$m, $\Delta\varphi = 3 \times 10^{-4}$. Fig.6 and 7 depict values of RMS displacement of the RO in horizontal (Fig.6) and vertical (Fig.7) planes along NESTOR orbit. Calculations were done for the values of RMS displacement and tilt of lattice elements equal to Δx, Δz, $\Delta s = 1 \times 10^{-4} m$, $\Delta xz, \Delta zs, \Delta sx$=$3 \times 10^{-4}\,rad$ (curves 1) and Δx, Δz, $\Delta s = 0.5 \times 10^{-4} m$, $\Delta xz, \Delta zs, \Delta sx$=$1 \times 10^{-4}\,rad$ (curves 2). It is clear from figures that maximum reference orbit displacements without correction in horizontal plane is in boundaries $\Delta x_{max} = 0.00144 - 0.00292\,m$, and in vertical plane $\Delta z_{max} = 0.00447 - 0.00871\,m$. Taking into account that NESTOR vacuum chamber sizes are $x = 0.03\,m$ to horizontal and $z = 0.03\,m$ to vertical, an injection can be done without preliminary correction procedures. Simultaneously, it is clear that the values of reference orbit displacements are big enough in both planes. This leads to essential increasing of an electron beam emittance, decreasing of the storage ring dynamic aperture and, therefore, decreasing of beam lifetime in the ring. Moreover, the values of RMS reference orbit displacement at the interaction point are in horizontal plane $x_{IP} = 0.0001272 - 0.0002578\,m$, and in vertical plane $z_{IP} = 0.0004629 - 0.0009412\,m$. Such values of electron and laser beam position mismatching essentially decrease effectiveness of the scattering process.

3. INJECTION CHANNEL

To provide parallelism of injection section of the ring with the linear accelerator axis the injection channel has to be parallel transition lattice with bending angles φ_{B1} and $\varphi_{B1} = -\varphi_{B2}$. We choose bending angle in the first magnet of the channel $\varphi_{B1} = 60°$. As base lattice for the transportation channel we used classical 5 lenses variant of the lattice [6], which has flexible focusing properties. Quadrupole lens doublet focuses the parallel electron beam in vertical plane in the center of the middle lens and gathers the electrons with different energies. In the horizontal plane, the parallel beam is focused in the middle of the section between the doublet and the middle quadrupole lens (the optimal place to install a collimator). The middle lens practically has no effect on particles with different energies and vertical trajectories but provide a possibility to change focusing characteristics of the channel in horizontal plane. Fig.8 shows the parallel electron beam trajectories in five lens objective.

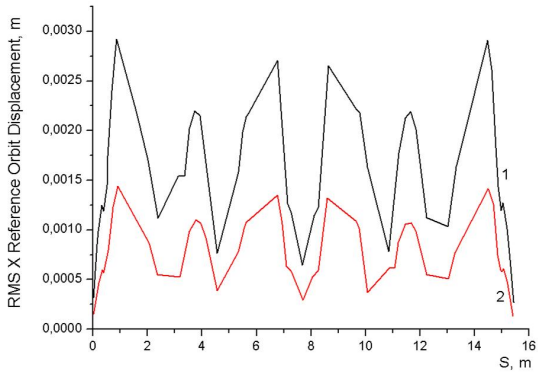

Fig.6. *RMS value of reference orbit displacement along NESTOR orbit in horizontal plane versus RMS value of lattice element alignment errors: 1 -* Δx,Δz,Δs=$1 \times 10^{-4} m$, $\Delta xz, \Delta zs, \Delta sx$=$3 \times 10^{-4}\,rad$; *2 -* Δx,Δz,Δs=$0.5 \times 10^{-4} m$, $\Delta xz, \Delta zs, \Delta sx$=$1 \times 10^{-4}\,rad$

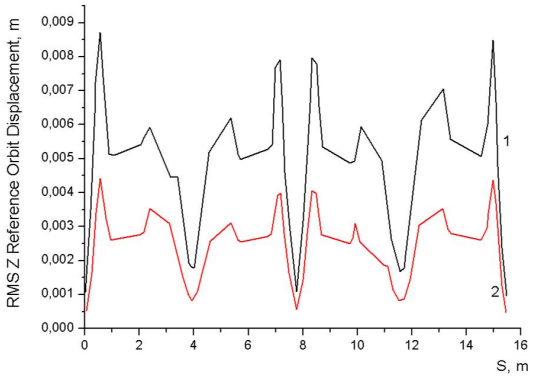

Fig.7. *RMS value of reference orbit displacement along NESTOR orbit in vertical plane versus RMS value of lattice element alignment errors: 1 -* Δx,Δz,Δs=$1 \times 10^{-4} m$, $\Delta xz, \Delta zs, \Delta sx$=$2 \times 10^{-4}\,rad$; *2 -* Δx,Δz,Δs=$0.5 \times 10^{-4} m$, $\Delta xz, \Delta zs, \Delta sx$=$1 \times 10^{-4}\,rad$

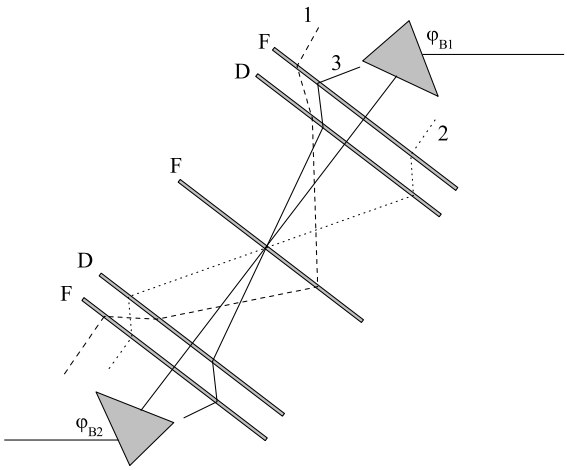

Fig.8. *Parallel electron beam trajectories in five lens objective: 1-horizontal beam size; 2-vertical beam size; 3-dispersion*

To provide the effective injection it is necessary to match the electron beam emittance at the end of the transportation channel and the storage beam acceptance. The source date for the calculations are parameters σ the matrix of an electron beam at the end of a linear acclerator $\sigma_x = \sigma_z = 1\,mm$, $\sigma_{x'} = \sigma_{z'} = 1\,mrad$ and parameters of σ the matrix that is determined by the storage ring phase ellipse that was transported back trough the bending magnet fringe field (Fig.9). In TRANSPORT code the tilts of ellipses are set with correlation coefficients

$$r_{ij} = \frac{\sigma_{ij}}{\sqrt{\sigma_{ii}\sigma_{jj}}},$$

where $\sigma_{11} = \epsilon_x\beta_x$, $\sigma_{22} = \epsilon_x/\gamma_x$, $\sigma_{21} = -\epsilon_x\alpha_x$ and the same expressions for the vertical plane. If we know the maximal ellipsoid sizes Y_{max}, Y'_{max} and its emittance we easy can get correlation coefficients for linear and angle coordinates from the expression $\beta\gamma - \alpha^2 = 1$: Signs + and − correspond to divergent and convergent beam respectively. At $X_{max} = 1.94\,mm$, $X'_{max} = 3.96\,mrad$ and $Z_{max} = 1.59\,mm$, $Z'_{max} = 1.69\,mrad$ (Fig.9) we have $r_{21} = -0.992$, $r_{43} = 0.928$.

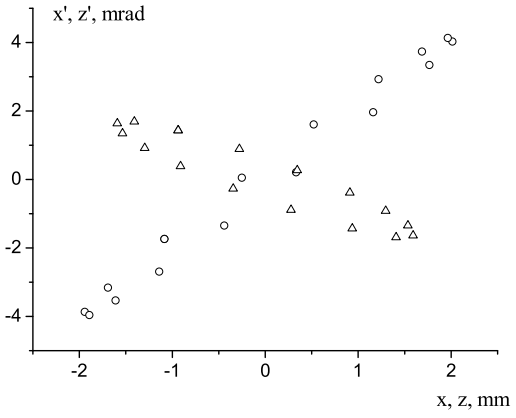

Fig.9. *Phase ellipse of the beam produced with beam transportation trough fringing field of the bending magnet*

The final part of the injection channel i.e. inflector, quadrupole of the storage ring and fringing field of the bending magnet is dispersion system. So, transportation channel has to compensate this dispersion. One can determine this dispersion by transportation of a particle with energy deviation in opposite direction from injection azimuth to the end of the magnetic screen. Calculations show that the parallel transition has to provide the dispersion equal to $D = 0.176\,m$ and its derivation $D' = -0.754$ at the magnetic screen exit In Fig.10 (1 for x, 2 for z) the results of the injection channel calculations for angles $\varphi_{B1} = 60°$, $\varphi_{B2} = -60°$ with focusing properties providing beam sizes matching are shown. As it can be concluded from the Fig.9 and Fig.10 comparison, injection channel provides electron beam transition with required beam parameters from the exit of the linear accelerator to the injection azimuth in the storage ring.

Fig.11 shows the electron beam envelopes and dispersion function in the calculated transportation channel. Fig.12 shows the layout of the transportation channel.

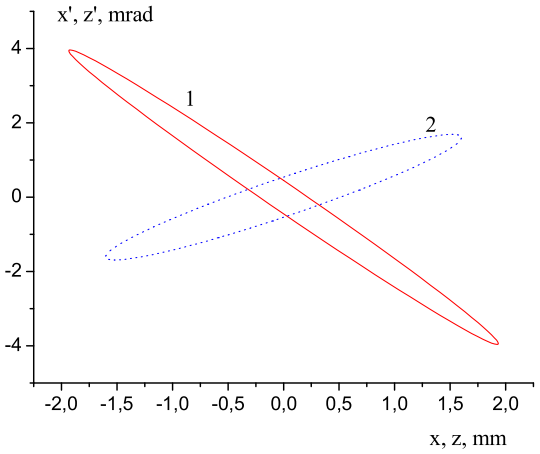

Fig.10. *Phase ellipse of the beam produced with beam transportation trough transportation channel*

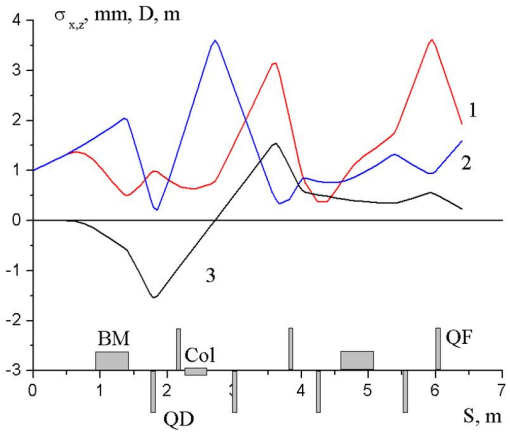

Fig.11. *The electron beam envelopes and dispersion function in the calculated transportation channel*

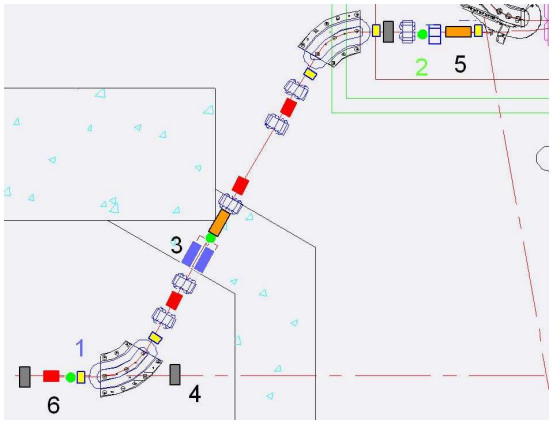

Fig.12. *NESTOR injection channel layout: 1 - bellows joint, 2 - pumping points, 3 - collimator, 4 - vacuum valve, 5 - beam position monitor, 6 - beam correctors*

The forces of the channel lenses are shown in Table1.

The dependence of the RO displacement due to power supply instability has been investigated. The calculations show that at power supply stability equal to $\Delta V/V$ up to 10^{-3} the RO displacements are inessential.

Table 1. *Quadrupole lens forces*

No	Q	K1
1	Q1	-0.07535
2	Q2	0.07356
3	Q3	-0.05537
4	Q4	0.06453
5	Q5	-0.02015
6	Q6	-0.04614
7	Q7	0.0622

In the same time, the small changes of the dispersion function were observed. It leads to the change of he beam envelopes of the channel. Fig.13 shows the transportation channel dispersion function at different values of the power supply instability. The maximum value of the dispersion function corresponds to $\Delta V/V = 10^{-3}$ of the power supply instability. As one can see from the figure, power supply instability will not have essential effect to the electron beam dynamics in the transportation channel.

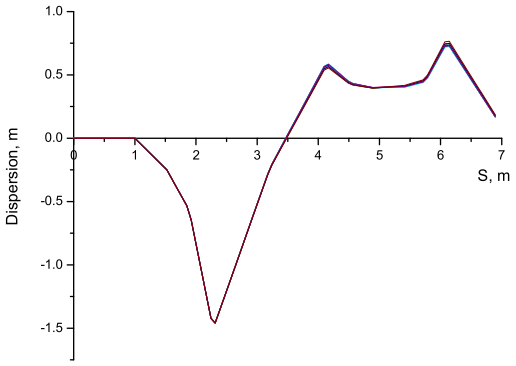

Fig.13. *Dispersion function of the NESTOR facility transportation channel at different value of the power supply instability: red curve for $\Delta V/V = 0$; blue for $\Delta V/V = 10^{-3}$*

To determine the value of the transportation channel magnetic element alignment tolerances the calculations have been carried out. Fig.14 shows the maximal displacements of the electron beam centroid line for two values of the transverse misalignment errors (100 and 200 μm) and two different values of element tilts (100 and 200 μrad). As one can see, the designed channel has stable focusing lattice. At 200 μm) value of tolerances the maximal value of the centroid displacement is not more then 3 mm. So, one can pass the electron beam trough the injection channel with element alignment errors of about 200 μm. But orbit correction will be needed to provide beam pass trough the collimator and accurate beam delivery to the injection region. Such correction was made with four pairs of correctors (see Fig.12). Fig.15 shows one variation of the centroid displacement with further its correction.

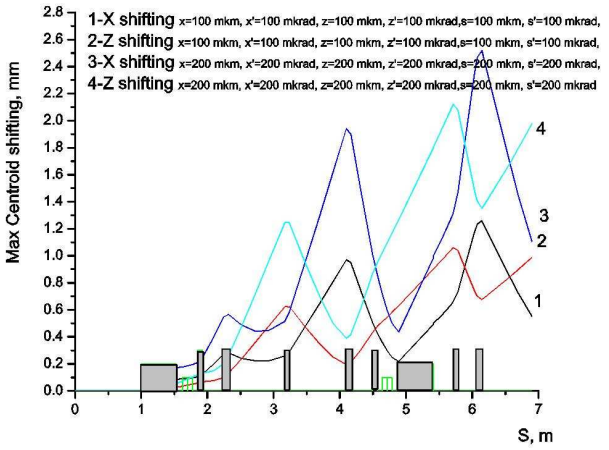

Fig.14. *The maximum value of the transportation channel electron beam centroid in dependence on element displacements*

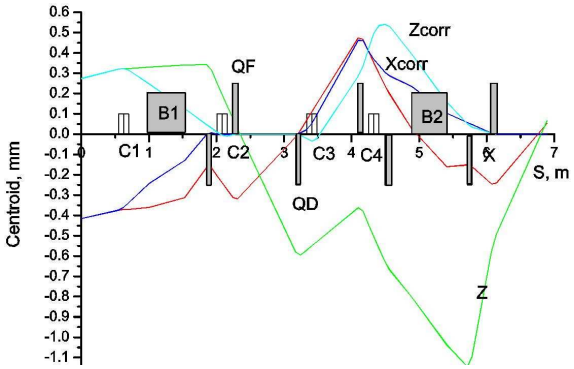

Fig.15. *The electron beam centroid displacement in the NESTOR facility transportation channel before and after correction (element misalignment are 200 μm and 200 μrad)*

Fig.16 shows the RMS value of the centroid displacement before and after beam position correction at 200 μm and 200 μrad misalignments. It is clear that proposed variant of correction can provided electron beam centroid correction.

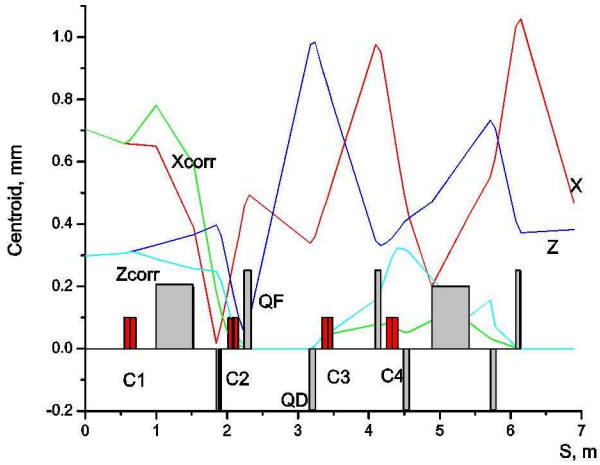

Fig.16. *The RMS electron beam centroid displacement in the NESTOR facility transportation channel before and after correction (element misalignment are 200 μm and 200 μrad)*

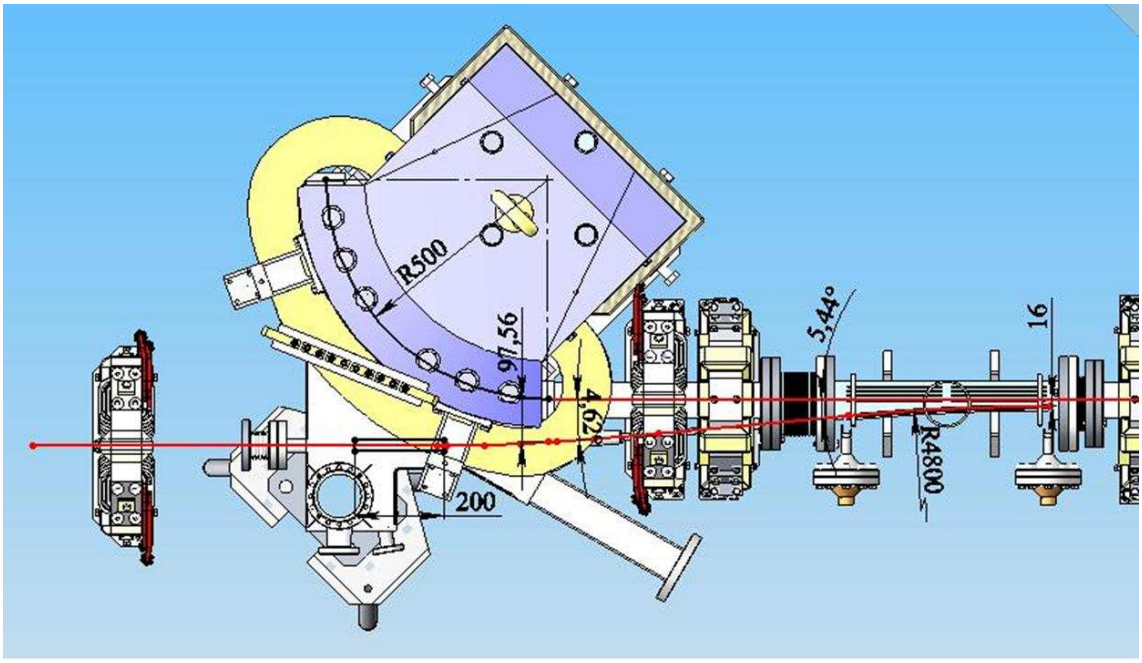

Fig.17. *Layout of the injection scheme of NESTOR storage ring*

4. INJECTION SCHEME

The layout of the electron beam injection scheme in the NESTOR storage ring is shown in Fig.17. Electron beam with energy of $\sim 60\,MeV$ from the injector (linear accelerator) trough transportation channel with parallel transition of the beam and final doublet of quadrupoles is delivered to the fringe field of a bending magnet. The effect of the magnetic field is reduced with magnetic screen. The magnetic induction of the fringe field along the beam trajectory is changed in the range between 500 and $600\,Gs$ of the magnetic field gradient in the magnet of $150\,Gs/cm$. This field deflects the beam to the reference orbit. Magnetic screen is made of soft steel like ARMCO and is tube with inner diameter of $10\,mm$ and outer diameter of $20\,mm$. The length of the screen is $200\,mm$. The reduction rate of the screen is 50. Position of the screen with respect to the bending magnet is shown in Fig.18.

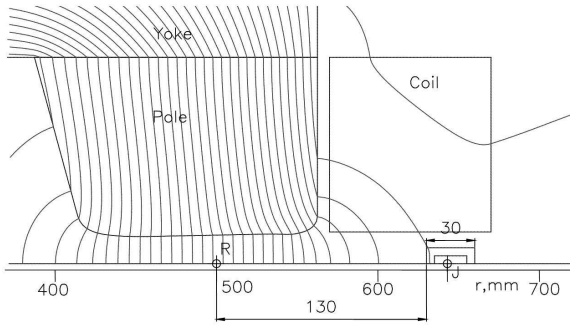

Fig.18. *Magnetic screen position in the transversal cross section of the injection bending magnet*

Such position of the magnetic screen was chosen taking into account the effect of the screen on the bending magnet field distribution. The location depicted in the Fig.2 leads to the local deviation of the field of about $\sim 5\,Gs$. This field change can be improved with a correction coil of the bending magnet. Effect of the screen on the magnetic field topography of the bending magnet is shown in Fig.19.

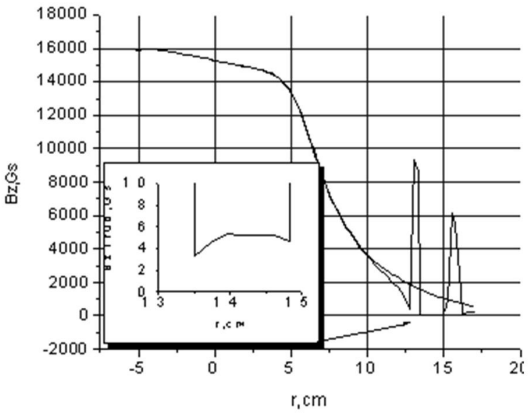

Fig.19. *Radial magnetic field distribution for maximal electron beam energy with and without magnetic screen. In insertion distribution of the field inside screen's tube is shown*

Further, the beam through quadrupole and sextupole of the storage ring lattice arrives to the entrance of an inflector. Passing through quadrupole magnet ($1.8\,T/m$ at injection energy) $0.0782\,m$ apart from reference orbit of the ring the beam is deflected on the 0.8° angle to the reference orbit. Magnetic field of the sextupole is weak and does not effect the injected beam trajectory. As a result, at the entrance of the inflector the beam has angle of 5.45° to the reference orbit and its distance from the reference orbit of the storage ring is $37.8\,mm$. In the inflector the beam moves along arc of $600\,mm$ length with radius of $4.8\,mm$. At the exit of the inflector the injected beam is in $16\,mm$ from the reference orbit under zero angle to the circulating beam. With damping time equal to $3\,sec$ the beam is injected to the reference orbit.

5. INFLECTOR

Starting from the parameters, that we should provide at the injection, we designed an electrical inflector. The operation of the inflector is based on the principle of the running wave [4]. The electrical circuit of the inflector operation with parameters is shown in Fig.20.

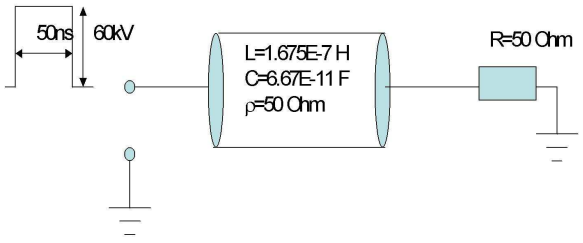

Fig.20. *The electrical circuit of the inflector operation with parameters*

The value of capacity $C = 6.67 \times 10^{-11} F$, inductivity $L = 1.675 \times 10^{-7} H$ and resistance $= 50\,\Omega$ can be changed depending on parameters of generator.
In Fig.21. the designed inflector is depicted.

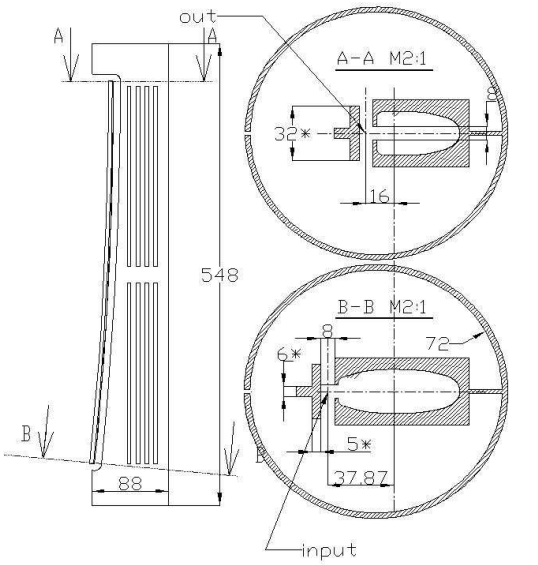

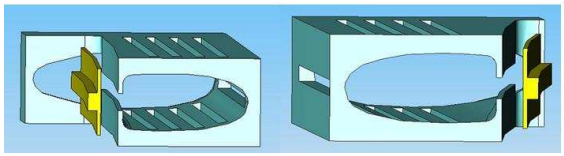

Fig.21. *Layout of the inflector on the base of the running wave*

The gap between septum electrodes is $8\,mm$. Voltage value at the anode is of about $60\,kV$. With impedance of inflector equal to $50\,\Omega$ the inflector current is of about $\sim 1200\,A$.
The size of the slot in the second electrode (cathode) is $8\,mm$ and was chosen from the condition of minimal inflector field at the storage ring reference orbit for providing acceptable lifetime of the circulating beam. With chosen geometry of the inflector the field at the reference orbit is of about 2.5% of the field in the inflector gap. It allows to carry out the injection with repetition of $0.1\,Hz$. The main parameters of the inflector, that determine requirement to the generator-power source of the inflector are presented in Table 2.

Table 2. *The main parameters of the inflector*

impedance, Ω	50
Deflection angle, $^\circ$	5.44
Pulse voltage, kV	60
Pulse current, A	1200
Pulse duration, $nsec$	50
Time of growth and drop, $nsec$ (no more)	5
Start synchronization, $nsec$	2
Pulse stability, %	1

Magnetic and electrical field distributions are shown in Fig.14.

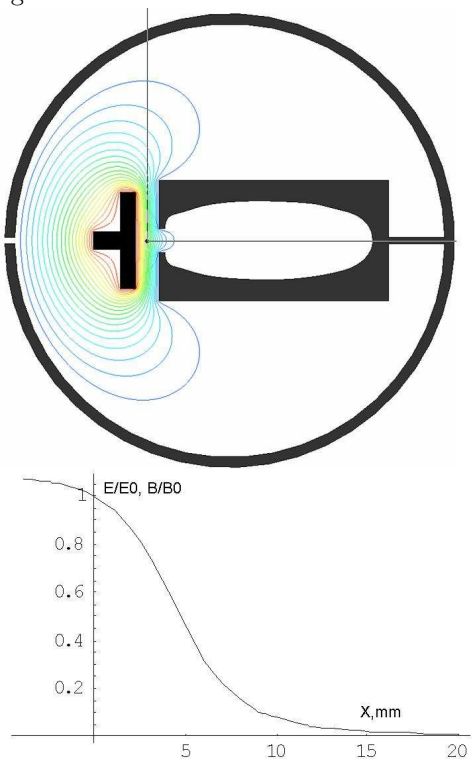

Fig.22. *Distribution of magnetic and electrical fields in the inflector on the base of running wave*

Below the components of magnetic and electrical fields in the gap of the designed inflector are presented:

$$B_x[T] = -0.88y - 3.5 \times 10^2 xy - 8 \times 10^4 x^2 y - 1.2 \times 10^7 x^3 y + 2 \times 10^4 y^3;$$

$$B_y[T] = 0.021 - 0.91x - 1.8 \times 10^2 x^2 - 2.5 \times 10^4 x^3 + 2.2 \times 10^2 y^2 + 7.2 \times 10^4 xy^2;$$

$$E_x[V/m] = 6.1 \times 10^6 - 2.6 \times 10^8 x - 5.2 \times 10^{10} x^2 - 7.2 \times 10^{12} x^3 + 6.5 \times 10^{10} y^2 + 2.1 \times 10^{13} xy^2;$$

$$E_y[V/m] = 2.5 \times 10^8 y + 9.9 \times 10^{10} xy + 2.3 \times 10^{13} x^2 y + 3.5 \times 10^{15} x^3 y - 5.8 \times 10^{12} y^3.$$

So, we can estimate focusing properties of the inflector fields.

6. SIMULATION OF PARTICLE MOTION

The particle tracing through the ring devices by integration of motion equations on a time in a crossed fields using equation system [7] was made. It allows to find out solution on any distance from a reference orbit where field is described. According to the results of calculations of beam dynamics from magnetic screen exit to the end of the inflector, the beam is focused in z direction and is defocused in x direction. Beam size in x direction is changed in 2...3 times. So, the horizontal size at the entrance of the inflector should be no more than $0.5\,mm$. For that the horizontal size at the entrance of the transportation channel should be no more than $0.2\,mm$ and accuracy of the beam position set is $0.1\,mm$.

Finally, beam sizes and its position at the entrance of the injection region will be formed with doublet of quadtrupoles depending on real distribution of the magnetic field in the injection bending magnet. This field distribution will be defined after magnetic measurements of the bending magnet.

7. CONCLUSIONS

The conceptual design of the NESTOR X-ray source transportation system is presented in the paper. The results of calculations show that presented injection system project provides the effective electron beam injection to the compact electron storage ring. Using the electric inflector on running wave it is possible to carry out the injection to the NESTOR ring through the fringing field of the dipole magnet.

References

1. E. Bulyak, P. Gladkikh, I.Karnaukhov, et al. Compact X-ray Source Based on Compton Backscattering // *Nucl. Inst. & Meth.* 2002, A487, p.241-248.

2. P. Gladkikh, A. Mytsykov, A. Ryezayev, A. Zelinsky. Investigation of injection through bending magnet fringe fields in X-rays source based on storage ring NESTOR // *European Particle Accelerator Conf.* Lucerne, Switzerland, 2004, p.1434.

3. P. Gladkikh, I. Karnaukhov, A. Mytsykov, A. Zelinsky. Injection system for Kharkov X-ray source NESTOR // *European Particle Accelerator Conf.* Edinburgh, Scotland, 2006, p.2038.

4. G.A. Mesyats. Semiconductor Opening Switch Research at IEP // *10-th IEEE International Pulsed Power Conf.* Albuquerque, USA, 1995, p.298.

5. V.Androsov, E.Bulyak, A.Dovbnya, et al. Progress in Development of Kharkov X-Ray Generator NESTOR // *Free Electron Laser Conf.*, Stanford, USA, 2005, p.476.

6. H. Wiedemann. *Particle Accelerator Physics I.* Berlin: "Springer", 1998, 472 p.

7. M. Szilgyi. *Electron and Ion Optics.* Moskow: "Mir", 1990, 639 p. (in Russian).

КОНЦЕПЦИЯ ИНЖЕКЦИИ УСТАНОВКИ *НЕСТОР*

П.И. Гладких, А.Ю. Зелинский, И.М. Карнаухов, А.О. Мыцыков, В.Л. Скирда

В течение последних лет в ННЦ ХФТИ создается источник рентгеновского излучения НЕСТОР. В соответствии с проектом 60 МэВ - электронный пучок инжектируется в накопительное кольцо и дальше может быть ускорен до максимальной энергии 225 МэВ. Поскольку магнито-оптическая структура накопительного кольца очень компактна, инжекционная траектория пучка проходит через рассеянное поле дипольного магнита накопителя НЕСТОР. Это вносит дополнительные трудности при разработке инжекционной системы. В статье представлена система инжекции установки НЕСТОР. Результаты разработок показывают, что спроектированная система обеспечивает согласование параметров инжектируемого пучка с аксептансом накопителя и устойчива к ошибкам установки элементов.

КОНЦЕПЦІЯ ІНЖЕКЦІЇ УСТАНОВКИ *НЕСТОР*

П.І. Гладких, А.Ю. Зелінський, І.М. Карнаухов, А.О. Мициков, В.Л. Скирда

Протягом останніх років у ННЦ ХФТИ створюється джерело рентгенівського випромінювання НЕСТОР. Згідно з проектом 60 МеВ - електронний пучок інжектується в нагромаджувач і далі може бути прискорений до максимальної енергії 225 МеВ. Оскільки магніто-оптична структура нагромаджувача дуже компактна, інжекційна траєкторія пучка проходе через розсіяне поле дипольного магніту нагромаджувача НЕСТОР. Це вносить додаткові труднощі при розробці інжекційної системи. В статті представлена система інжекції установки НЕСТОР. Результати розробок показують, що спроектована система забезпечує узгодження параметрів пучка, який інжектується, з аксептансом нагромаджувача та стійка до помилок встановлення елементів.